AIMS Materials Science, 12(4): 861–876.
DOI: 10.3934/matersci.2025037
Received: 24 May 2025
Revised: 29 July 2025
Accepted: 06 August 2025
Published: 29 August 2025

https://www.aimspress.com/journal/Materials

Research article

Enhancing corrosion resistance of Ti6Al7Nb alloy using nano bioactive ceramic coating by EPD in biomedical applications

Anmar Tallal Kadhim[1], Ayad Naseef Jasim[1], Alaa A. Atiyah[2] and Abbas Al-Bawee[1]

[1] College of Engineering, University of Diyala, Baquba, Iraq
[2] Ministry of Higher Education and Scientific Research, Iraq

* **Correspondence:** Email: abbas_taha_eng@uodiyala.edu.iq; Tel: +964-7711031981.

Abstract: In this work, using the electrophoretic deposition (EPD) technique, Ti6Al7Nb alloy samples were coated with hydroxyapatite (HA) nanoparticles to enhance corrosion behavior and biological characteristics. In the absolute ethanol EPD suspension solution, hydroxyapatite concentrations varied at 2, 5, and 8 g/L, with chitosan as a binder. The EPD process potential was 40 V, the distance between the two electrodes was 1 cm, and the coating period was 4 min for all samples. X-ray diffraction (XRD). Scanning electron microscopy (SEM), and energy dispersive of X-ray (EDX) were used to test the coated sample. Corrosion behavior was also tested by measuring the open circuit potential (OCP) and polarization curve (Tafel). The wettability contact angle and adhesion tests were also measured. The optimum sample, coated with hydroxyapatite at 8 g/L, was immersed in simulated body fluid (SBF) for 1 month, and tested by XRD, SEM, and EDX. The results show that the corrosion rate was reduced 13 times, from 5.544×10^{-4} millimeters per year (mmpy) to 7.100×10^{-3} mmpy for the uncoated sample, and protection efficiency reached 92.19%. After immersion in SBF for 1 month, XRD and SEM results showed the appearance of a new hydroxyapatite layer with agglomerated particles, and the Ca/P ratio of 2.143 was close to the standard original ratio in the human body, an indicator for excellent osseointegration. The corrosion rate reached 2.841×10^{-4} mmpy, and the protection efficiency reached 96%, as an indicator of enhanced corrosion characteristics after immersion in SBF solution.

Keywords: Ti6Al7Nb alloy; electrophoretic deposition technique; hydroxyapatite (HA); corrosion behavior

1. Introduction

Titanium and its alloys can be used in biomedical applications [1], being attractive because of their mechanical properties, such as low Young's modulus and high corrosion resistance, their non-toxic and low allergenic properties, and their high osseointegration characteristics. These features make them good alternatives to other metals and alloy counterparts [2–4]. An example is Ti6Al7Nb, an alloy with a Young's modulus of approximately 100–110 GPa, lower than that of stainless steel (316L), which has a Young's modulus of 193 GPa, and of cobalt chrome alloy, which has a Young's modulus of 250 ± 10 GPa. This shows the enhanced biocompatibility of the Ti6Al7Nb alloy [5–7].

Researchers also seek to increase the bone osseointegration of titanium and its alloys by coating them with biocompatible materials such as hydroxyapatite [$Ca_{10}(PO_4)_6(OH)_2$, HA]. This is a significant bone composition component, besides collagen, as shown in Figure 1. It can increase the concentration of local Ca^{2+}, activating the proliferation of osteoblasts and promoting the growth and differentiation of mesenchymal stem cells (MSCs) [8–10]. Many techniques have been used for coating titanium and its alloys with hydroxyapatite, such as electrophoretic deposition (EPD), dip coating, plasma spray, and thermal spray [11,12]. In this work, hydroxyapatite was coated on a Ti6Al7Nb alloy using EPD to increase its osseointegration characteristics and enhance corrosion behavior. We used the chitosan (CS) as a binder and applied 4 V with a 2 cm distance between the Ti6Al7Nb alloy as the cathode and the stainless steel 316L as the anode, during a 44 min period X-ray diffraction (XRD). Scanning electron microscopy (SEM), and energy dispersive of X-ray (EDX) were applied to test the coated samples, and the wettability contact angle and adhesion were also tested. The behavior was also tested using a potentiostat to measure open circuit potential (OCP) and polarization curve (Tafel).

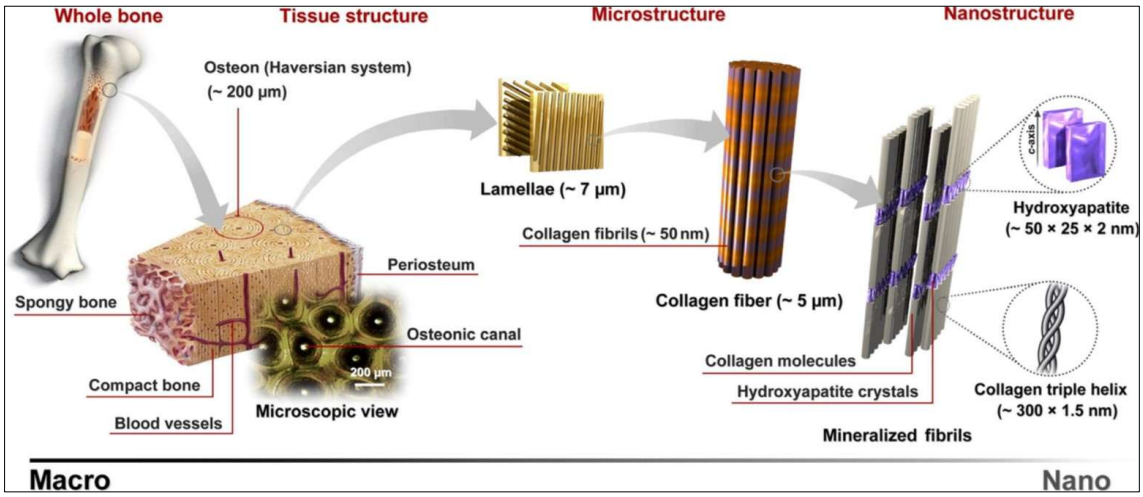

Figure 1. Hydroxyapatite in bone structure (Reproduced from Ref. [13] with permission).

This study offers a systematic analysis of hydroxyapatite coatings deposited on Ti6Al7Nb alloy using the EPD technique (with conventional chitosan as binding agent). The novelty of this study lies in the optimization of hydroxyapatite concentration in the ethanol-based suspension to reduce corrosion rate and improve biological performance. Unlike previous studies, a long immersion with SBF and a post-deposition heat treatment were used here to study the apatite reformation, chemically

verify the Ca/P ratio, and inspect the overall stability of the coating surface. A significant reduction in corrosion rate after long immersion with high protection efficiency confirms that the coating approach for the Ti alloy is suitable for biomedical applications.

2. Materials and methods

A Ti6Al7Nb alloy 100 mm rod was purchased from Bojijinsheng Metal Material Co., China, with the chemical composition shown in Table 1. The Ti6Al7Nb alloy was cut using a wire cutter machine into circular and semicircular samples with 2 mm thickness. The samples were ground using SiC grinding paper (p220–400–1000–2000) and cleaned twice with acetone (Sigma-Aldrich, USA) using an ultrasonic cleaner bath (1800 QT, China).

Table 1. Chemical composition (wt.%) of the Ti6Al7Nb alloy.

Al	Nb	Fe	C	H	O	N	Ti
6.0	7.1	0.19	0.018	0.005	0.08	0.024	balanced

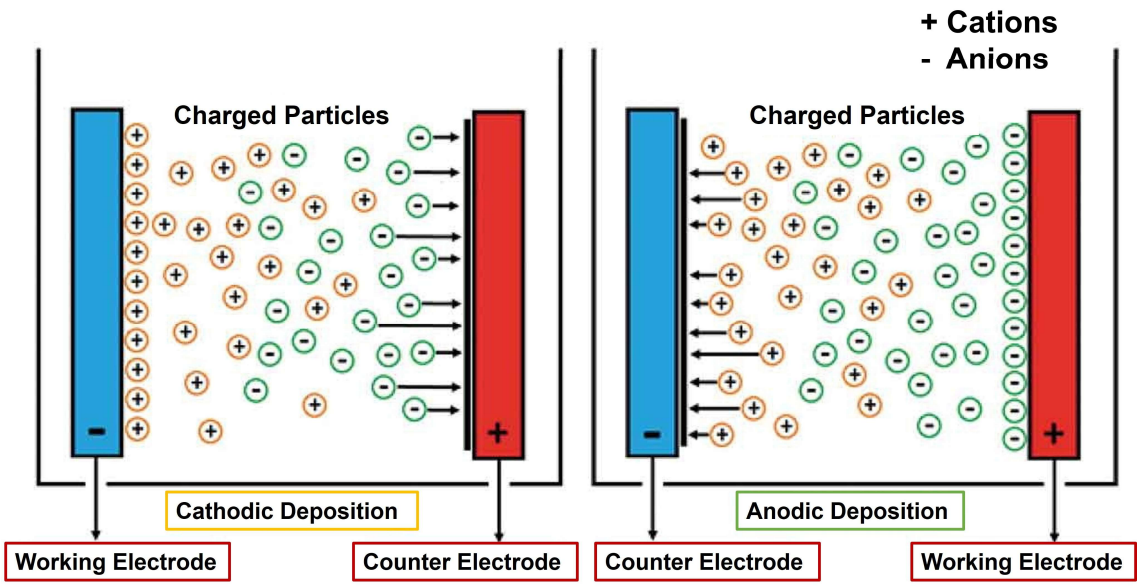

Figure 2. Schematic diagram for the electrophoretic deposition process (EPD) (Reproduced from Ref. [14] with permission).

The coating solution was prepared by dissolving 0.03 g of chitosan (purity 95.7%, ≤80 nm particle size, Hongwu International Group, China) in 1 mL of deionized water until it was disbanded. Then, 24 mL of ethanol 96% (CDH, India) was added to make up the total volume to 25 mL, and the solution was thoroughly mixed using a hot plate with a magnetic stirrer (VS-130SH, Korea). After that, 0.05 g of hydroxyapatite (≤40 nm particle size, Sky Spring nanomaterials, USA) was added to the solution to obtain a 2 g/L concentration; the solution was mixed on a hot plate with a magnetic stirrer. Then, the suspension solution was placed in an ultrasonic bath for 30 min to disperse the particles. The EPD process was performed by placing the Ti6Al7Nb alloy in the suspension solution and connecting it to the power supply (GPR-3060D, Taiwan) as a cathode; a stainless-steel plate 316L

acted as the anode, as shown in Figure 2. The potential used in EPD was 40 V, the distance between the two electrodes was 2 cm, and the coating period was 4 min. The EPD process was repeated with a changed hydroxyapatite concentration from 5 to 8 g/L. Coated samples were air dried and tested by XRD, SEM, and EDX. Also, an adhesion test and wettability contact angle were performed. A corrosion test was also performed on the samples using a potentiostat (CHI 604E, China) in simulated body fluid (SBF) as the corrosion media, to test the open circuit and a polarization curve (Tafel). After evaluation of the results, the optimum sample was immersed in SBF solution for one month and then heat-treated at 400 °C for 1 h. After immersing the sample, XRD was conducted to test it. SEM, EDX, and a corrosion test were also applied to compare the results before and after immersing in the SBF solution.

3. Results

3.1. XRD test

Figure 3a shows the XRD pattern for the Ti6Al7Nb alloy. There is a perfect match with the titanium standard identification card (JCPDS# 00-040-1294). Figure 3b represents the sample coated with a 2 g/L HA concentration. Hydroxyapatite peaks with a small intensity are visible, which match JCPDS# 01-086-0740, and many titanium peaks with a more significant intensity. This indicates that the Ti6Al7Nb alloy was coated with a thin hydroxyapatite layer. Figure 3c shows the hydroxyapatite peak intensity increase and titanium peak intensity reduction as indicators of a thicker coated layer for the 5 g/L hydroxyapatite concentration. Figure 3d shows the dominant hydroxyapatite peaks in the XRD pattern of the sample with 8 g/L of coating. The titanium peaks were reduced to a minimal intensity, indicating a good coverage of the coating layer.

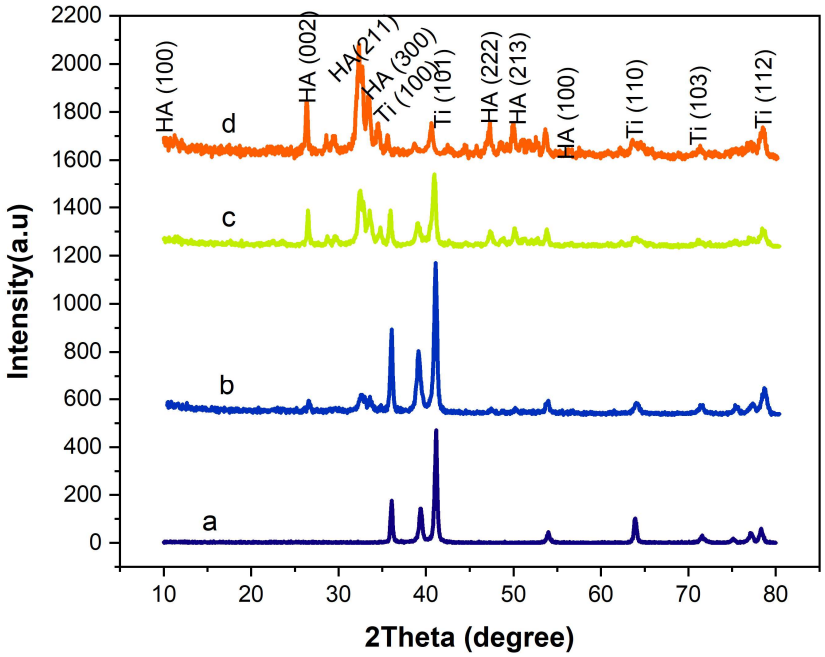

Figure 3. XRD patterns of uncoated samples and samples coated with 2, 5, and 8 g/L of HA Ti6Al7Nb.

3.2. Evolution of surface morphology in HA-coated Ti6Al7Nb alloys as observed by SEM

Figure 4 shows the SEM test images for all samples at different magnifications. Figure 4a,b shows the uncoated sample, and the Figure 4c,d shows the uniform coating of samples coated with 2 g/L HA; however, the coated layer shows many cracks in the coating. Figure 4e,f shows the sample coated with 5 g/L HA, which also presents a uniform coating but fewer cracks than those with 2 g/L HA, with the larger magnification image showing a large agglomeration in the coating layer. Figure 4g,h shows the sample coated with 8 g/L HA: there is uniform coating and no cracks, but the coating was very porous. Also, the larger magnification image shows a massive agglomeration. The thickness of the coating layers for HA concentrations of 2, 5, and 8 g/L was 36.57, 44.79, and 53.12 µm, respectively, as shown in Figure 5a–c. This explains the XRD test pattern: the peaks of hydroxyapatite intensity were elevated with increasing hydroxyapatite concentration.

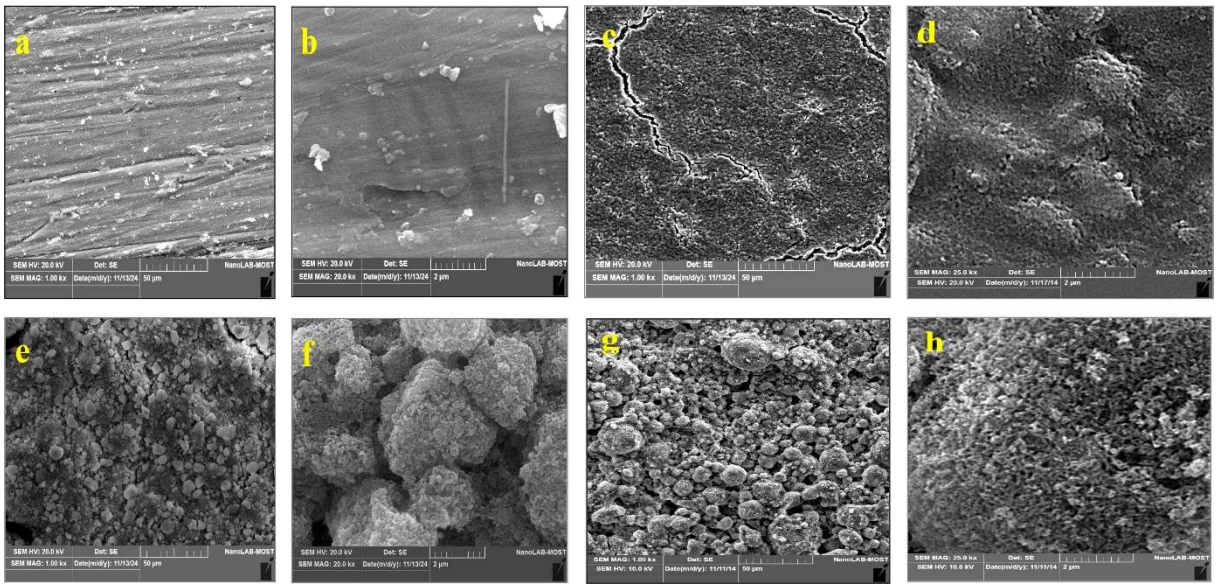

Figure 4. SEM images at different magnifications for (a, b) uncoated Ti6Al7Nb alloy, (c, d) 2 g/L HA-coated sample, (e, f) 5 g/L HA-coated sample, and (g, h) 8 g/L HA-coated sample.

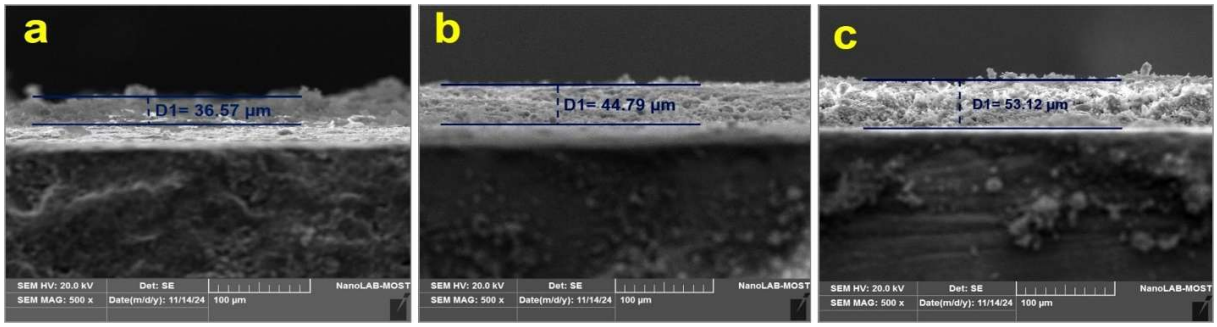

Figure 5. SEM test thickness images for (a) 2 g/L, (b) 5 g/L, and (c) 8 g/L of HA-coated samples.

3.3. EDX test

As depicted in Table 2, the EDX analysis shows clear distinctions between the uncoated and HA-coated Ti6Al7Nb alloys. This table shows the elemental makeup of the uncoated alloy, with clear peaks for titanium (Ti), aluminum (Al), and niobium (Nb), recorded at 85.92, 6.71, and 7.37 wt%, respectively. These values are consistent with the nominal composition obtained from the supplier, suggesting that the alloy's surface is pure and has maintained its integrity. Samples coated with 2, 5, and 8 g/L HA all present significantly lower concentrations of Al, Ti, and Nb when compared with the uncoated alloy, due to the HA coating covering the surface. For the other concentrations (2, 5, 8 g/L), the observed EDX spectrum of the Ti6Al7Nb sample does not show the metallic parts of the alloy, as they are completely covered by the HA layer; this is evident in the absence of the characteristic elements (Ti, Al, and Nb). For 2 g/L, the main elements detected in this sample were calcium at 38.48 wt%, phosphorus at 16.46 wt%, and oxygen at 42.73 wt%, the result of a normal additive for hydroxyapatite [$Ca_{10}(PO_4)_6(OH)_2$]. The small ratios correspond to the Na, Mg, Si, Fe, and Cl elements shown in Table 2. may be due to the impurities of residuals from HA synthesis. The results show that the 8 g/L HA coating creates a uniform and dense coating on the alloy surface, inhibiting any surface metallic elements.

Table 2. EDX test for uncoated and coated samples.

Element (wt%)	Uncoated	2 g/L	5 g/L	8 g/L
O	-	28.34	42.73	36.51
Na	-	0.60	0.33	0.50
Mg	-	0.18	0.18	0.14
Al	6.71	3.78	0.14	2.15
Si	-	0.12	0.24	0.08
P	-	2.95	16.46	7.38
Ca	-	5.78	0.22	15.32
Ti	85.92	53.62	38.48	20.64
Fe	-	0.63	-	0.41
Nb	7.37	4.01	1.23	3.01
Total	100.00	100.00	100.00	100.00

3.4. Electrochemical analysis and corrosion behavior

The 8 g/L HA-coated sample achieved −0.270 V at the OCP test, compared with −0.663 V by the uncoated sample, as shown in Figure 6 and Table 3. Passivation increased with increasing hydroxyapatite concentration.

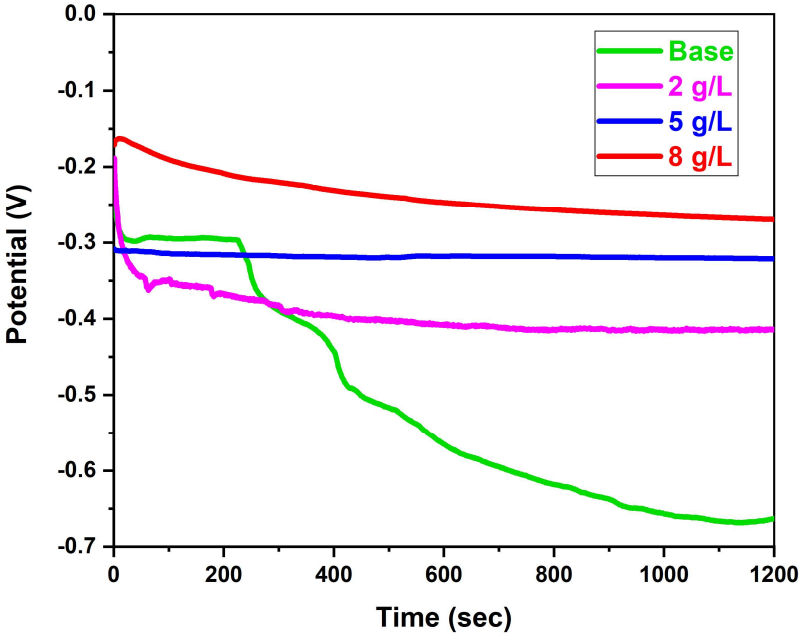

Figure 6. OCP test for all uncoated and coated samples.

Table 3. OCP test parameters for the uncoated and coated samples.

Sample	OCP (V)
Base	–0.663
2 g/L	–0.415
5 g/L	–0.321
8 g/L	–0.270

The corrosion rate for the sample coated with 8 g/L of hydroxyapatite was 5.544×10^{-4} mmpy, compared with 7.100×10^{-3} mmpy for the uncoated sample, translating into a reduction of about 13 times. The protection efficiency, calculated from Eq 1, shows that the protection efficiency for the 8 g/L HA-coated sample increased to 92.19%, as shown in Table 4. The polarization curve (Tafel) test shows that the corrosion rate decreases with increasing hydroxyapatite concentration, as shown in Figure 7 and Table 5 [15].

$$\text{Protection efficiency} = \frac{Iuncoated - Icoated}{Iuncoated} \times 100\% \quad (1)$$

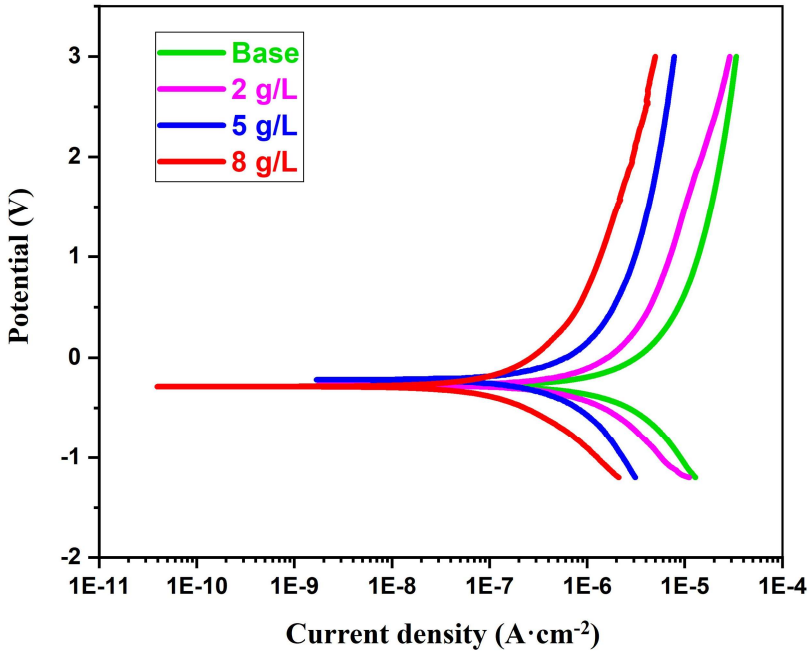

Figure 7. Polarization curve (Tafel) test for uncoated and coated samples.

Table 4. Corrosion characteristics for all coated samples.

Sample	E corr. (V)	I corr. (A)	Corr. rate (mmpy)	Protection efficiency (%)
Base	–0.294	8.172×10^{-7}	7.100×10^{-3}	-
2 g/L	–0.288	4.423×10^{-7}	3.842×10^{-3}	45.87
5 g/L	–0.205	1.718×10^{-7}	1.492×10^{-3}	78.28
8 g/L	–0.278	6.381×10^{-8}	5.544×10^{-4}	92.19

The polarization resistance, calculated from Eq 2, also increases with increasing HA concentration. The sample coated with 8 g/L HA achieved 696,432.9 Ω·cm^2, compared with 53,926.4 Ω·cm^2 for the uncoated sample, as shown in Table 5 [16,17].

$$Rp = \frac{\beta c \beta a}{2.303(\beta c \beta a) i_{corr.}} \quad (2)$$

Rp is the resistance of polarization (ohm·cm^2), βc and βa are the cathodic Tafel slope and anodic Tafel slope, respectively, and I_{corr} is the corrosion current density (A/cm^2).

Table 5. Resistance of polarization for all coated samples.

Sample	$I_{corr.}$ (Amp.)	Rp (Ω·cm^2)
Base	8.172×10^{-7}	53,926.4
2 g/L	4.423×10^{-7}	103,311.8
5 g/L	1.718×10^{-7}	264,749.0
8 g/L	6.381×10^{-8}	696,432.9

3.5. Wettability (contact angle test)

The wettability of uncoated and coated Ti6Al7Nb samples was evaluated through the contact angle measurements (Figure 8, Table 6). A contact angle of 84.25° for the Ti6Al7Nb uncoated base alloy indicates hydrophobic behavior. The alloy leaves little room for interaction with water due to a native oxide layer formed on titanium alloys. It is known that titanium alloys form an oxide layer that reduces interaction with aqueous media; still, hydrophilic behaviors could be found to some extent, as would be the case in nature. In samples coated with 2 g/L HA, the contact angle reduced to 55.85°, indicating better wettability due to HA introducing more water interactions. This change in contact angle behavior can occur if HA particles create a hydrophilic surface structure with polar functional groups upon contact with the surface. Coating with 5 g/L led to a contact angle of 34.95°, indicating stronger hydrophilic properties than the previous samples. The contact angle was reduced as the thicker and denser HA layer creates a denser surface that increases water interaction areas due to increased surface roughness. The phosphate and hydroxyl groups of the HA particles are hydrophilic in nature and thus induce strong surface water attraction properties. The contact angle measurement on the 8 g/L HA-coated sample presented near-super-hydrophilic behavior with values below 5°. The measured SEM images outline a thick, porous HA layer that allows water to penetrate and spread due to capillary effects and high surface energy. The HA's increased surface roughness and porosity lead to deeper water absorption and interaction, which can ultimately lower the contact angle, in accordance with the Wenzel and Cassie-Baxter model for wetting on rough surfaces. Increasing surface hydrophilicity occurs with increasing levels of HA concentration. A desirable improvement in wetting properties is noted, as it increases cell adhesion, proliferation, and bonding of the implant to the surrounding bone. Ultimately, the increase in surface hydrophilicity with HA content also decreases the contact angle, demonstrating that HA coating can improve the estimated bioactivity of Ti67Al7Nb implants.

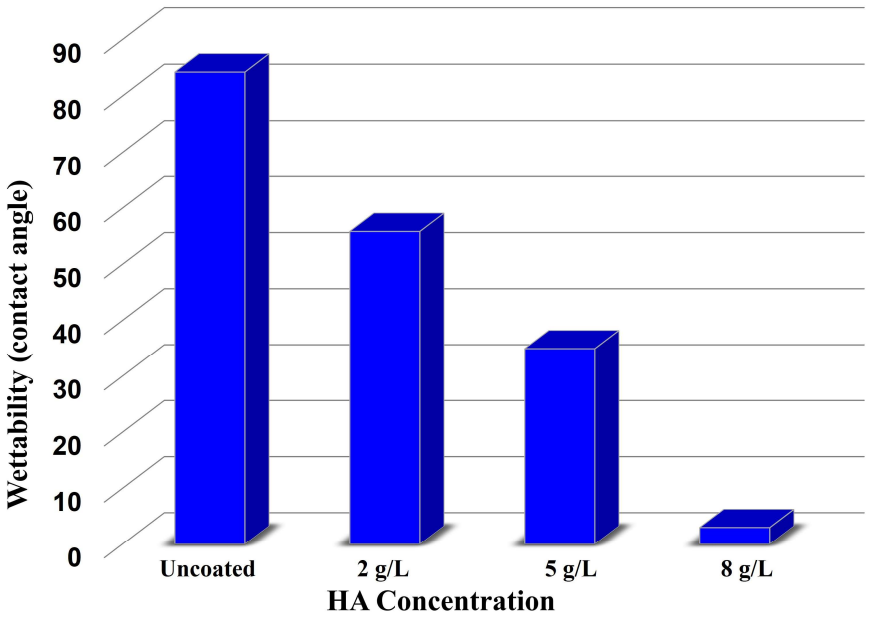

Figure 8. Wettability (contact angle) test for all samples.

Table 6. Wettability (contact angle) values for all samples.

Sample	Contact angle (°)
Base	84.25 ± 3
2 g/L	55.85 ± 2
5 g/L	34.95 ± 4
8 g/L	<5 ± 1

3.6. Adhesion test

The adhesion test, shown in Figure 9 and Table 7, which was performed according to the ASTM D3359 standard test, shows that adhesion increased with increasing HA concentration. This is due to HA increasing the adhesion of the chitosan polymers, which play the role of a binder, to the coating layer. In fact, their classification became more excellent with the increase in concentration.

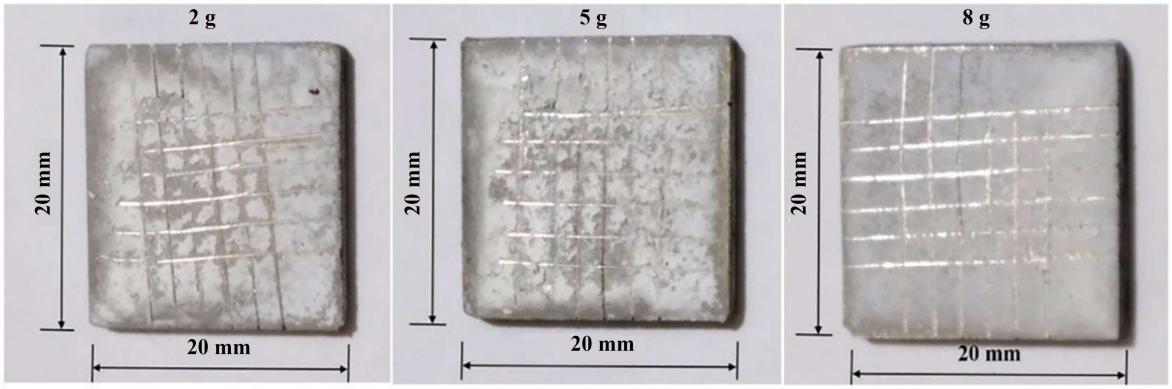

Figure 9. Adhesion test for coated samples.

Table 7. Adhesion test values for coated samples.

Classification	Percent area removed (%)	Sample
1B	36	2 g/L
2B	16	5 g/L
4B	1	8 g/L

3.7. Zeta potential measurement

The zeta potential increased with increasing concentrations of HA in the suspension solution, as shown in Figure 10.

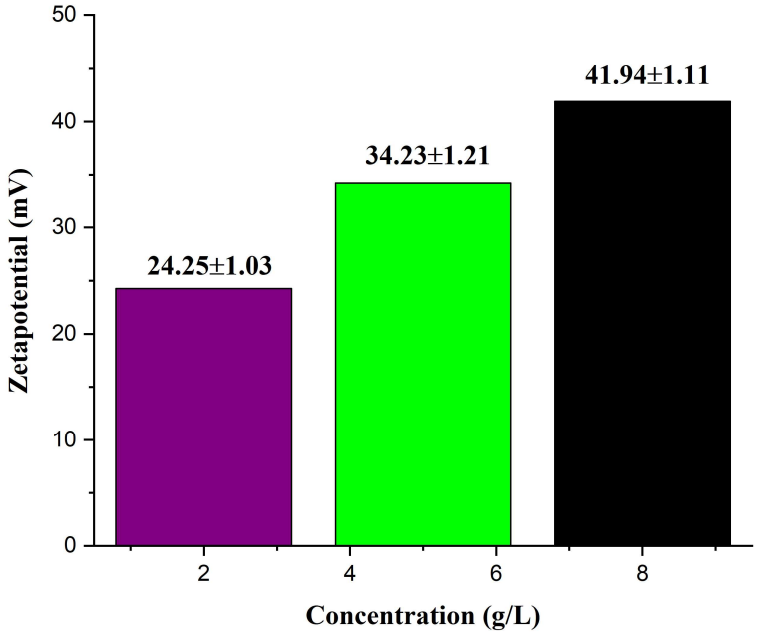

Figure 10. Zeta potential variation with hydroxyapatite concentration.

3.8. After immersion in SBF solution for one month

3.8.1. XRD test after immersion in SBF solution

The XRD test of the optimum sample (8 g/L HA concentration) after immersion in SBF solution for 1 month is shown in Figure 11. Hydroxyapatite peaks appear with higher intensity than before immersion (Figure 3d). The HA peaks were a perfect match (JCPDS# 01-086-0740), explained by a new HA layer naturally forming from the SBF solution on the surface of the 8 g/L HA coating layer. This is a good indicator for the osseointegration of coated samples.

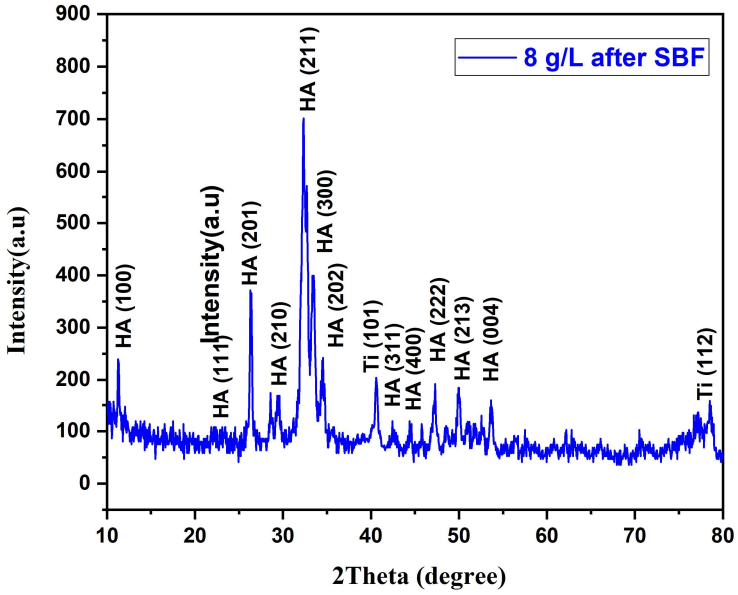

Figure 11. XRD pattern of the 8 g/L HA-coated sample after immersion in SBF for one month.

3.8.2. SEM test after immersion in SBF solution

The SEM images of the 8 g/L HA-coated sample after immersion in SBF solution (Figure 12a,b) show agglomerated spherical hydroxyapatite particles covering all sample surfaces. This is an indicator of the sample's osseointegration ability. Because of particle agglomeration, the particle size varied from 64 to 120 nm.

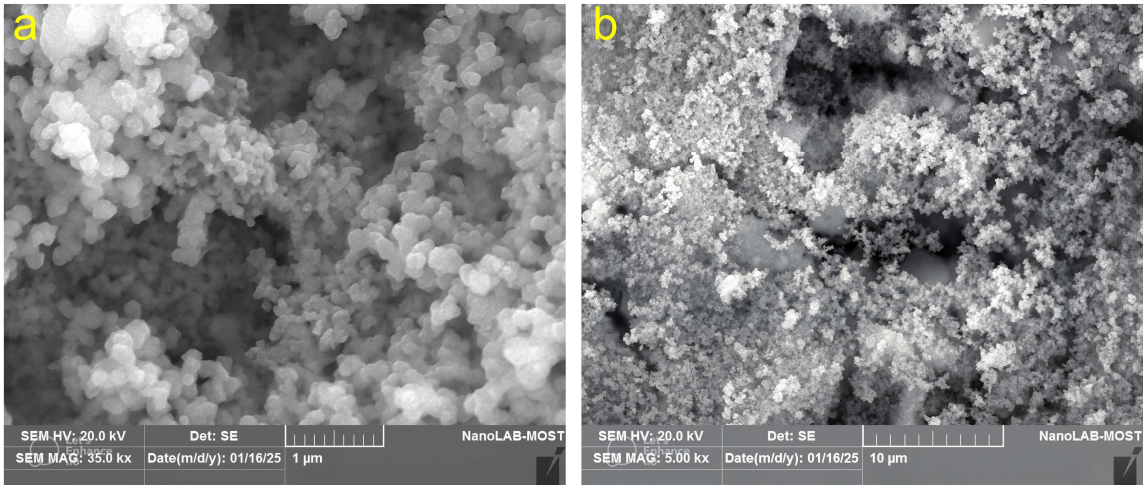

Figure 12. SEM images of the 8 g/L HA-coated sample after immersion in SBF for one month.

3.8.3. EDX test after immersion in SBF solution

The EDX elemental analysis of the 8 g/L HA-coated sample after immersion in SBF solution for 1 month shows the appearance of a hydroxyapatite component [$Ca_{10}(PO4)_6(OH)_2$] and some minerals present in the SBF solution, like Na, Mg, K, Cl, and S, as shown in Table 8. The Ca/P ratio was 2.143, very close to the original standard weight ratio, which was 2.156; i.e., the former hydroxyapatite was very close to the natural hydroxyapatite in the human body.

Table 8. EDX test elemental analysis of the 8 g/L HA-coated sample after immersion in SBF for one month.

Element	wt%
O	33.32
Na	11.45
Mg	2.66
P	11.47
S	0.67
Cl	14.10
K	1.42
Ca	24.58
Ti	0.12
Total	100.00

3.8.4. Corrosion test after immersion in SBF solution

The corrosion behavior improved after 1 month of immersing the 8 g/L HA-coated sample. The OCP test value increased to −0.12 from −0.27 V before immersion, i.e., the sample was more passive, as shown in Figure 13. Also, corrosion rate decreased from 5.544×10^{-4} to 2.841×10^{-4} mmpy after immersion, as shown in Table 9 and Figure 14. This happened because the new hydroxyapatite layer formed from the SBF solution blocked most of the porosity in the coated layer, further hindering the solution from reaching the sample's surface.

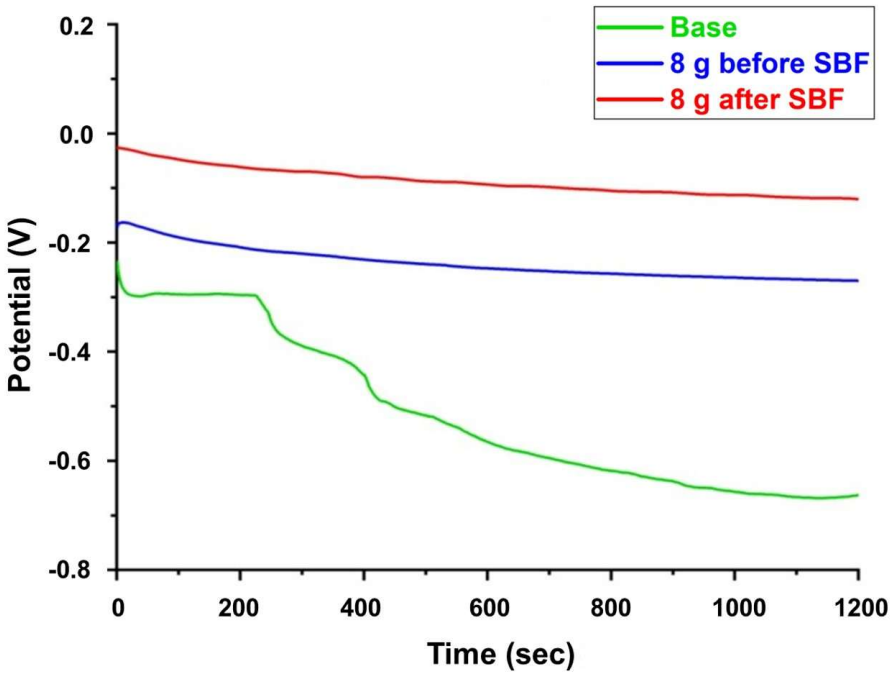

Figure 13. OCP comparison of the 8 g/L HA-coated sample before and after immersion in SBF for one month.

Table 9. Corrosion characteristics for the 8 g/L HA-coated sample before and after immersion in SBF for one month.

Sample	$E_{corr.}$ (V)	$I_{corr.}$ (A)	Corr. rate (mmpy)	OCP (V)
8 g/L	–0.278	6.381×10^{-8}	5.544×10^{-4}	–0.270
8 g/L after SBF	–0.515	3.270×10^{-8}	2.841×10^{-4}	–0.120

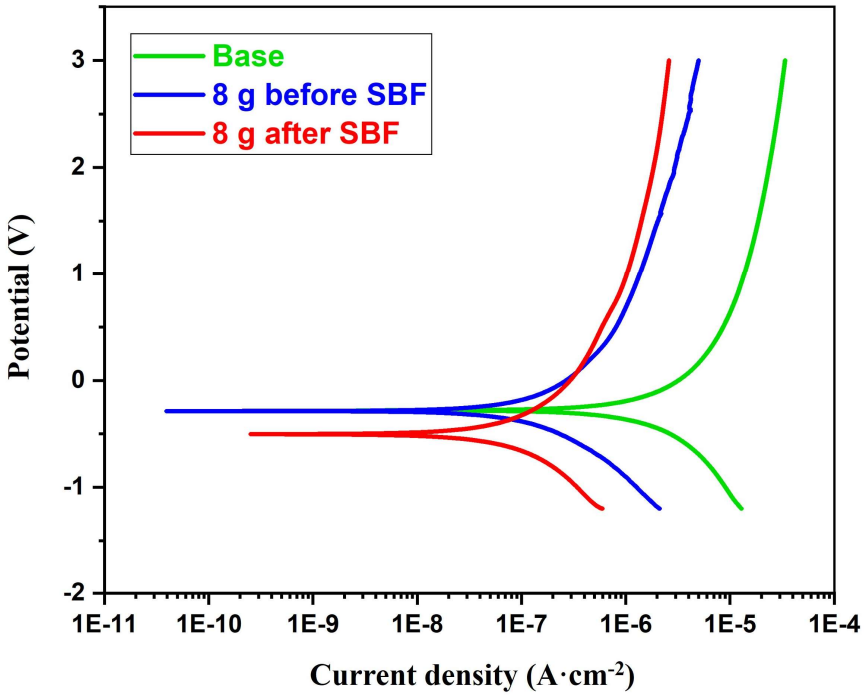

Figure 14. Polarization curve (Tafel) of the 8 g/L HA-coated sample before and after immersion in SBF for one month.

The protection efficiency, calculated from Eq 1, increased to 96% after immersion, compared with 92.19% before immersing. All this ensures the enhancement of corrosion characteristics after 1 month of immersion in SBF solution.

3.8.5. Hypothesis

It is predicted that increasing the amount of HA in HA/bioactive glass (BG) hybrid coatings will improve the initial corrosion resistance of the Ti-6Al-7Nb substrate by enhancing the compactness, crystallinity, and barrier effects of the coatings. However, increased concentration of HA in the coatings may have a negative impact on long-term stability in biological environments, since HA has a limited release of ions and apatite regeneration compared to BG, not to mention that HA-rich formulations have less bioactivity. HA concentration requires a trade-off between short-term protection and long-term bioactivity.

4. Conclusions

This study proved that EPD can successfully apply a HA coating to Ti-6Al-7Nb substrates. In summary, the study showed that:

1. XRD showed that the coating quality improves with increasing concentrations of HA applied on Ti6Al7Nb substrates after an EPD coating process. The XRD pattern shows the 2 g/L coating had weak HA peaks, while the 5 and 8 g/L coatings resulted in a stronger HA peak and lowered Ti peaks, suggesting greater thickness, crystallinity, and surface coverage.

2. SEM supported that greater HA concentrations improved the uniformity of the coatings, with fewer cracks at the surface, and a better bond to the Ti6Al7Nb substrate. The surface changed from being cracked and with sparse coverage at 2 g/L HA to a denser layer of HA and no cracking at 8 g/L. The coating thickness increased throughout the concentration range, from 36.57 μm (2 g/L) to 44.79 μm (5 g/L), and finally to 53.12 μm (8 g/L HA).

3. The electrochemical corrosion analysis of Ti6Al7Nb alloys showed that corrosion performance improved dramatically with increasing HA coating concentration. The uncoated metal had an OCP of −0.663 V; HA coatings at 2, 5, and 8 g/L had OCP values of −0.415, −0.321, and −0.270 V, respectively, which significantly improved surface passivation.

4. The corrosion current density (I_{corr}) varied from 8.172×10^{-7} A in uncoated samples to 4.423×10^{-7} A with 2 g/L HA, 1.718×10^{-7} A with 5 g/L HA, and 6.381×10^{-8} A with 8 g/L HA. This indicates decreasing corrosion activity. Similarly, the corrosion rate changed from 7.100×10^{-3} mmpy for the uncoated alloy to 5.544×10^{-4} mmpy for the 8 g/L HA-coated sample, which reduced the degradation rate.

5. The adhesion tests supported that an increased HA concentration increases the bonding of coatings to Ti6Al7Nb substrates. At 2 g/L HA, 36% of the area was removed (1B rating), indicating weak bonding. At 5 g/L HA, we observed 16% removal (2B), and the 8 g/L HA-coated sample could only remove 1%, for a strong 4B rating.

6. Finally, in the 8 g/L HA-coated Ti6Al7Nb sample as compared to the baseline, there was improved corrosion resistance, after a period of one month submersion in SBF. OCP improved from –0.270 to –0.120 V, and the corrosion rate decreased by nearly 50% (from 5.544×10^{-4} to 2.841×10^{-4} mmpy) due to the formation of a secondary HA layer. This resulted in increased efficiency of protection from 92.19% to 96%, improving passivation and healing of the surface.

Use of AI tools declaration

The authors declare they have not used Artificial Intelligence (AI) tools in the creation of this article.

Author contributions

Anmar Tallal Kadhim: writing-original draft, funding acquisition, conceptualization; Ayad Naseef Jasim: writing-review & editing, visualization; Alaa A. Atiyah: validation, formal analysis; Abbas Al-Bawee: project administration and methodology supervision and investigation.

Conflict of interest

The authors declare no conflict of interest.

References

1. Marin E, Lanzutti A (2024) Biomedical applications of titanium alloys: A comprehensive review. *Materials* 17: 114. https://doi.org/10.3390/ma17010114
2. Kumar A, Gori Y, Kumar A, et al. (2022) *Advanced Materials for Biomedical Applications*, Boca Raton: CRC Press. https://doi.org/10.1201/9781003344810

3. Leyens C, Peters M (2006) *Titanium and titanium alloys: Fundamentals and applications*, 2 Eds., Weinheim: WILEY-VCH. https://doi.org/10.1002/3527602119
4. Jung HD (2022) Titanium and its alloys for biomedical applications. *Metals* 11: 1945. https://doi.org/10.3390/met11121945
5. Ashida M, Chen P, Doi H, et al. (2014) Microstructures and mechanical properties of Ti-6Al7Nb processed by high-pressure torsion. *Procedia Eng* 81: 1523–1528. https://doi.org/10.1016/j.proeng.2014.10.184
6. Balijepalli S, Donnini R, Kaciulis S, et al. (2013) Young's modulus profile in Kolsterized AISI 316L steel. *Mater Sci Forum* 762: 183–188. https://doi.org/10.4028/www.scientific.net/MSF.762.183
7. Al-Bawee A, Khodair Z, Hussein K, et al. (2024) Enhancing biocompatibility and osseointegration of medical implants using Ti-based nanocomposite coatings. *Multidiscip Sci J* 6: 2024183. https://doi.org/10.31893/multiscience.2024183
8. Pokhrel S (2018) Hydroxyapatite: Preparation, properties and its biomedical applications. *Adv Chem Eng Sci* 8: 225–240. https://doi.org/10.4236/aces.2018.84016
9. Fiume E, Magnaterra G, Rahdar A, et al. (2021) Hydroxyapatite for biomedical applications. *Ceramics* 4: 542–563. https://doi.org/10.3390/ceramics4040039
10. Shi H, Zhou Z, Li W, et al. (2021) Hydroxyapatite based materials for bone tissue engineering: A brief and comprehensive introduction. *Crystals* 11: 149. https://doi.org/10.3390/cryst11020149
11. Fotovvati B, Namdari N, Dehghanghadikolaei A (2019) On coating techniques for surface protection: A review. *J Manuf Mater Process* 3: 28. https://doi.org/10.3390/jmmp3010028
12. Tsygankov A, Skryabin S, Krikorov A, et al. (2019) Formation of a combined bioceramics layer on titanium implants. *J Phys Conf* 1386: 012011. https://doi.org/10.1088/1742-6596/1386/1/012011
13. Fathi Kazerooni A, Pozo JM, McCloskey EV, et al. (2020) Diffusion MRI for assessment of bone quality: A review of findings in healthy aging and osteoporosis. *J Magn Reson Imaging* 51: 975–992. https://doi.org/10.1002/jmri.26973
14. Priyadarshini B, Rama M, Chetan, et al. (2019) Bioactive coating as a surface modification technique for biocompatible metallic implants: A review. *J Asian Ceram Soc* 7: 397–406. https://doi.org/10.1080/21870764.2019.1669861
15. Al-Saadie KAS, Al-Mashhdani HAY (2015) Corrosion protection study for carbon steel in seawater by coating with SiC and ZrO_2 nanoparticles. *Am J Chem* 5: 28–39. http://article.sapub.org/10.5923.j.chemistry.20150501.05.html
16. Al-Bawee A, Khodair Z, Hussein A (2025) Impact of surface titanium alloy coatings for biomedical applications. *AIP Conf Proc* 3282: 020015. https://doi.org/10.1063/5.0265031
17. Makurat-Kasprolewicz B, Wekwejt M, Pezzato L, et al. (2024) Effect of ultrasound on the physicochemical, mechanical and adhesive properties of micro-arc oxidized coatings on Ti13Nb13Zr bio-alloy. *Sci Rep* 14: 25421. https://doi.org/10.1038/s41598-024-75626-4

AIMS Press